
Article:
Kimura, A., Yamauchi, Y., Hodono, S. et al. (5 more authors) (2017) Treatment response of ethyl pyruvate in a mouse model of chronic obstructive pulmonary disease studied by hyperpolarized129Xe MRI. Magnetic Resonance in Medicine, 78 (2). pp. 721-729. ISSN 0740-3194

https://doi.org/10.1002/mrm.26458

Treatment response of ethyl pyruvate in a mouse model of chronic obstructive pulmonary disease studied by hyperpolarized ^{129}Xe MRI

Journal:	*Magnetic Resonance in Medicine*
Manuscript ID	MRM-16-16948.R1
Wiley - Manuscript type:	Full Paper
Date Submitted by the Author:	n/a
Complete List of Authors:	Kimura, Atsuomi Yamauchi, Yukiko Hodono, Shota Stewart, Neil; University of Sheffield, Unit of Academic Radiology Hosokawa, Osamu Hagiwara, Yu Imai, Hirohiko Fujiwara, Hideaki
Research Type:	Hyperpolarized imaging < Technique Development < Technical Research, Translational Research < Physiological Research
Research Focus:	Pathology < Function < Other tissues (body fluids, skin, vessels, arteries, other organs, etc)

Treatment response of ethyl pyruvate in a mouse model of chronic obstructive pulmonary disease studied by hyperpolarized ^{129}Xe MRI

Atsuomi Kimura,*[1] Yukiko Yamauchi,[1] Shota Hodono,[1] Neil James Stewart,[2] Osamu Hosokawa,[1] Yu Hagiwara,[1] Hirohiko Imai,[3] and Hideaki Fujiwara[1]

[1] Department of Medical Physics and Engineering, Division of Medical Technology and Science, Faculty of Health Science, Graduate School of Medicine, Osaka University

[2] Academic Unit of Radiology, University of Sheffield, Sheffield, South Yorkshire, UK

[3] Research and Educational Unit of Leaders for Integrated Medical System, Center for the Promotion of Interdisciplinary Education and Research, Kyoto University, Kyoto, Japan

Running head:

HPXe MRI of murine COPD model and therapy response

Word count: 4492

*Corresponding author: Atsuomi Kimura, PhD, Department of Medical Physics and Engineering, Division of Medical Technology and Science, Faculty of Health Science, Graduate School of Medicine, Osaka University, 1-7 Yamadaoka, Suita, Osaka 565-0871, Japan,

Phone: +81-6-6879-2478, E-mail: kimura@sahs.med.osaka-u.ac.jp

ABSTRACT

Purpose: To investigate disease progression and treatment response in a murine model of chronic obstructive pulmonary disease (COPD) using a preclinical hyperpolarized ^{129}Xe (HPXe) MRI strategy.

Methods: COPD phenotypes were induced in 32 mice by 10 weeks of exposure to cigarette smoke (CS) and lipopolysaccharide (LPS). The efficacy of ethyl pyruvate (EP), an anti-inflammatory drug, was investigated by administering EP to 16 of the 32 mice after 6 weeks of CS and LPS exposure. HPXe MRI was performed to monitor changes in pulmonary function during disease progression and pharmacological therapy.

Results: HPXe metrics of fractional ventilation and gas-exchange function were significantly reduced after 6 weeks of CS and LPS exposure compared to sham-instilled mice administered with saline ($P < 0.05$). After this observation, EP administration was started in 16 of the 32 mice and continued for 4 weeks. EP was found to improve HPXe MRI metrics to a similar level as in sham-instilled mice ($P < 0.01$). Histological analysis showed significant alveolar tissue destruction in the COPD group, but relatively normal alveolar structure in the EP and sham-instilled groups.

Conclusion: This study demonstrates the potential efficacy of EP for COPD therapy, as assessed by a non-invasive, translatable ^{129}Xe MRI procedure.

Abstract word count: 200

Keywords: Hyperpolarized ^{129}Xe MRI, lung functional assessment, murine chronic obstructive pulmonary disease, treatment response, ethyl pyruvate

INTRODUCTION

Chronic obstructive pulmonary disease (COPD), a heterogeneous lung disease characterized by both chronic airway inflammation and emphysematous alveolar tissue destruction, is predicted to be the third leading cause of death worldwide by 2020 (1). At present, pharmacological therapies for COPD have shown limited efficacy and thus the development of new therapeutic drugs is vital for improving patient outcomes (2). The use of appropriate animal models of COPD that adequately induce the key symptoms of the disease is indispensable for therapy development, and rodent models are especially important. In particular, preclinical studies with mice are often appropriate because a wide range of well-characterized disease models is available (3,4). As smoking and repeated lung infections are the primary causes of COPD, several murine COPD models have been developed by exposing mice to cigarette smoke. Despite certain models showing good reproducibility for inducing the two main phenotypes of COPD mentioned above, the lack of applicable methods for assessment and diagnosis of these disease models remains a limiting factor for preclinical studies. Most previous studies have relied on plethysmography and/or histology to evaluate the applicability of murine COPD models, necessitating a tracheostomy and/or mouse death for each examination (5,6) and hence making it difficult to evaluate drug efficacy repetitively and longitudinally. To help resolve this problem, non-invasive imaging techniques that allow the longitudinal assessment of disease progression and therapeutic efficacy of drugs in vivo are required.

MRI using hyperpolarized (HP) noble gases (^{3}He and ^{129}Xe) as contrast agents offers an attractive means to visualize and quantitatively evaluate pulmonary functional parameters such as ventilation and gas-exchange (7-9). In a number of studies in small animals and humans, pathological changes of these fundamental

parameters have been investigated using HP gas MRI and quantitative measures of ventilation and gas-exchange dysfunction caused by COPD have been established (10,11). HP ^{129}Xe (HPXe) is a versatile contrast agent to evaluate drug efficacy in the lungs because it allows not only imaging of ventilation, but also the assessment of pulmonary gas-exchange, thanks to its solubility in pulmonary tissues and blood. To this end, we have developed a continuous-flow mode polarizer for HPXe production and have established non-invasive MRI procedures under spontaneous respiration for the assessment of pulmonary function in mice (12,13). In this study, we apply our HPXe methodology to explore the feasibility of a new drug for COPD therapy.

Ethyl pyruvate (EP), an anti-inflammatory agent, is a candidate for pharmacological therapy of COPD. In recent years, EP has been shown to demonstrate therapeutic efficacy in various animal models of lung diseases, such as acute lung injury (ALI) and pulmonary arterial hypertension (PAH) (15-17). The therapeutic efficacy of EP is attributed to its ability to regulate high-mobility group box protein-1 (HMGB1) release from innate immune cells, and to deactivate subsequent cytokine production that would further stimulate inflammatory responses (18,19). HMGB1, which is an abundant chromatin protein, may play a crucial role in pharmacological therapy of COPD because it is known to not only trigger inflammatory responses but also, paradoxically, to activate cells involved in tissue repair (20-24). HMGB1 functions by binding with the receptor for advanced glycation end products (RAGE) and Toll-Like Receptors 2 and 4. In recent years, it has been shown that HMGB1 can also initiate wound healing processes through binding with RAGE followed by activation of the extracellular signal-regulated kinase 1/2 (ERK1/2) signaling pathway (23). RAGE is expressed in pulmonary tissues with relatively high basal levels (22), and EP has been reported to activate the ERK1/2 signaling pathway (14). Thus, EP

shows considerable potential as a drug for lung tissue repair accompanied with anti-inflammatory responses through regulation of the HMGB1/RAGE pathway.

In the present study, we demonstrate the observation of disease progression in a mouse model of COPD induced by cigarette smoke (CS) exposure and lipopolysaccharide (LPS) instillation, as measured by HPXe MRI. Additionally, the efficacy of ethyl pyruvate (EP) for treatment of this COPD model is studied to assess the feasibility of this non-invasive imaging technique as a diagnostic method for early disease detection and therapy response evaluation in COPD.

METHODS

Animal preparation

Thirty-seven male, 6-week-old, type ddY mice, weighing 30 – 35 g (Japan SLC, Inc., Shizuoka, Japan) were included in this study. All experimental procedures and animal care standards conformed to Osaka University guidelines. Mice were divided into two groups: a sham-instilled group of N=5 mice and a CS and LPS group of N=32. The CS and LPS mice were further divided into 2 equal groups of 16 individuals. The two subgroups were separately administered with a combination of CS and LPS as follows. CS of approximately 2.1 L in volume resulting from one cigarette (Lark Milds: tar 9 mg, nicotine 0.8 mg; Philip Morris International Inc., New York, USA) was collected into a Tedlar® bag (Sigma-Aldrich, St Louis, MO, USA). The mice in each subgroup were placed in a semi-sealed plastic container with a volume of 12.4 L and 9 airshafts of 5 mm inner diameter on its upper surface. CS was flowed from the Tedlar® bag into the container for 26 minutes at a rate of 40 mL/min. Following this, fresh room air was flowed into the container for 5 minutes (at 720 mL/min). This whole-body exposure

procedure was performed twice daily on five consecutive days within one week, and repeated on a weekly basis as described below. On each fifth day, a 20 µL solution of LPS in saline (0.4 mg/kg, LPS in *Escherichia coli*, serotype O55:B5, Sigma-Aldrich, St. Louis, MO, USA) was delivered intra-tracheally to the mice at least 2 hours prior to the CS exposure. The sham-instilled mice were intra-tracheally administered with 20 µL of saline on every fifth day in the same manner as the LPS administration.

Six weeks after commencing CS and LPS exposure, the two subgroups of CS and LPS mice were assigned as follows: a pure CS and LPS group of N=16 mice and an EP-treated group of N=16 mice. For the pure CS and LPS group, the same protocol of CS and LPS administration was continued for a further 4 weeks. EP-treated mice were intra-tracheally administered with a 20 µL solution of EP in saline (1.3 mg/kg, Tokyo Chemical Industry Ltd, Tokyo, Japan) on a daily basis for 4 weeks, in addition to the continued administration of CS and LPS as detailed above. EP was always administered after the CS and LPS exposure, separated by an interval of at least 2 hours. Therefore, in total, 10 weeks were required to completely prepare the CS and LPS, and EP-treated groups. The sham-instilled mice were intra-tracheally administered with 20 µL of saline per day, every weekday, for this 4 week period, in the same manner as the EP treatment. The survival rates of the whole 10-week procedure were 75% for CS and LPS mice (12 out of 16 mice survived), 75% for EP-treated mice (12 out of 16 mice survived), and 100 % for the sham-instilled group.

In all cases, prior to the instillation of saline, LPS or EP solution, mice were anesthetized with 2% isoflurane (ISOFLU®, Dainippon Sumitomo Pharmaceutical Co. Ltd, Osaka, Japan), which was administered via a nose cone using a home-built anesthesia system connected to an isoflurane vaporizer (Isorex I-200, Shin-Ei

Industries, Inc., Tokyo, Japan). Subsequently, mice were intubated with a 22 G catheter (SURFLO® F&F, Terumo Corp., Tokyo, Japan) while positioned supine and secured to a slanted wooden board, and then the saline, LPS or EP solution was instilled.

MR measurements of sham-instilled and CS and LPS groups were performed at 0 weeks (prior to the first administration) and 2, 6, 8 and 10 weeks after commencing the administration of CS and LPS. Similarly, MR measurements of the EP-treated group were performed at 0, 6, 8 and 10 weeks after commencing the administration of CS and LPS (i.e. -6, 0, 2 and 4 weeks from commencement of EP therapy). Immediately before all MR measurements, mice were anesthetized with 2% isoflurane as detailed above. A plastic mouth mask, to which three polyethylene tubes were connected (for HPXe gas delivery, O_2 delivery and exhaled gas exhaust), was attached to the animal prior to placement in the MR scanner. In order to synchronize image acquisitions with respiratory motion, a pulse transducer (AD Instruments Ltd., Dunedin, New Zealand) was positioned on the mouse abdomen, just inferior to the diaphragm. This sensor converted the respiratory motion into an electrical signal that was monitored in real-time using LabVIEW software (National Instruments, Austin, TX, USA). The animal's body temperature in the magnet was maintained with warm water circulating through a rubber tube placed on the abdomen. The MR imaging procedure was performed without tracheal intubation or tracheotomy and hence was entirely non-invasive.

^{129}Xe Polarization and Gas Delivery

^{129}Xe nuclei were polarized to ~10% by Rb-^{129}Xe spin-exchange optical pumping (25) with a home-built continuous-flow ^{129}Xe polarizer (26). A gas mixture consisting of 70% Xe (natural abundance, comprising 26% ^{129}Xe) and 30% N_2 was supplied from a pre-mixed cylinder (Air Liquid Japan Ltd., Tokyo, Japan) at a pressure of 0.15 atmospheres for ^{129}Xe polarization. Once polarized, HPXe was subsequently compressed to atmospheric pressure with a diaphragm pump (LABOPORT® N86 KN.18, KNF Neuberger GmbH, Freiburg, Germany) to facilitate gas delivery directly and continuously from the polarizing cell to the mouse in the magnet. The HPXe gas mixture was flowed continuously at a rate of 50 mL/min to each mouse and was mixed with O_2 (continuously supplied at 9 mL/min) in the mouth mask. The percentages of Xe and O_2 spontaneously inhaled by the mice were 59.3% and 15.3%, respectively.

MR Imaging

All MR measurements were performed on a Agilent Unity INOVA 400 WB high-resolution NMR spectrometer system running VNMR 6.1C software (Varian Inc., Palo Alto, CA, USA). A 9.4 T vertical magnet with a bore width of 89 mm (Oxford Instruments Plc., Oxford, UK) was used. A self-shielded gradient probe was employed in combination with Litz volume RF coils of 34 mm inner diameter, tunable to the Larmor frequencies of ^{129}Xe (110.6 MHz) and ^{1}H (399.6 MHz) (Clear Bore DSI-1117, Doty Scientific, Inc., Columbia, SC, USA).

For assessment of pulmonary ventilation and gas-exchange function, HPXe gas images were acquired with a 2D multi-shot balanced steady-state free precession (bSSFP) sequence, which was programmed in-house (27). Acquisition parameters were as follows: RF pulse, 1000 μs long Gaussian-shaped pulse with a bandwidth of 2800 Hz and centered on the ^{129}Xe gas-phase resonance (0 ppm); TR/TE, 3.2/1.6 ms;

receiver bandwidth, 62 kHz; one coronal slice of thickness 20 mm, covering the whole of the lungs; matrix size, 64 × 32; field of view, 80 × 25.6 mm^2; number of shots (required to fill k-space), 4; flip angle, 40º; number of averages of the whole acquisition, 8; centrically-ordered phase encoding. ^{129}Xe images were reconstructed by a 2D fast Fourier transform after zero filling to a 128 × 64 matrix using in-house MATLAB scripts (MathWorks Inc., Natick, MA, USA).

Evaluation of ventilation function

For evaluating pulmonary ventilation function, the fractional ventilation (i.e. the fraction of gas "turned over" per breathing cycle), r_a, was mapped across the lungs following a previously reported method (28,29). Briefly, after the HPXe concentration in the lungs had reached a steady-state under the continuous supply of HPXe and O_2, two pre-saturation RF pulses were applied at the ^{129}Xe gas-phase frequency to destroy any gas-phase ^{129}Xe magnetization in the alveoli. The bSSFP imaging sequence was then used to acquire respiratory-synchronized ^{129}Xe gas ventilation images at inspiration after *n* breathing cycles. The value of *n* was sequentially incremented from 1 to 10, and then to 12, 15 and 20; thus, thirteen ^{129}Xe ventilation images were acquired in total. (In Reference (28), images were acquired after 1 to 10 breaths only; the purpose of the additional acquired images here was to improve the accuracy of the r_a estimate.) From the resulting image series, the fractional ventilation of each voxel was evaluated by analyzing the dependency of the ^{129}Xe MR signal intensity upon the number of breaths (Equations 2 and 3, Reference (28)). The fractional ventilation, r_a, is defined as:

$$r_a = \frac{V_f}{V_o + V_f}, \qquad [1]$$

where V_o and V_f denote the volumes of old and new (fresh) gas within the voxel after each breath, respectively. r_a values were determined pixel-by-pixel over the whole image to derive a r_a map, and averaged for each mouse to obtain the whole lung r_a. Finally, the whole lung r_a values were averaged for each of the sham-instilled, CS and LPS, and EP-treated groups to obtain group mean r_a values.

Evaluation of gas-exchange function

The efficiency of HPXe gas-exchange between the alveoli (gas-phase) and the lung parenchyma and capillaries (dissolved-phase) was evaluated by the xenon polarization transfer contrast (XTC) method (30). Briefly, a XTC image was generated by acquiring bSSFP gas ventilation images at expiration, separated by the application of four frequency-selective inversion pulses (inter-pulse delay 20 ms) at the Larmor frequency of dissolved-phase ^{129}Xe (197 ppm), and comparing the resulting ventilation image intensities (27). The flip angle of the inversion pulse (Gaussian-shape; 1000 μs duration) was calibrated prior to the present study. Similarly, a "control" bSSFP image was generated by acquiring ventilation images at expiration, separated by the application of the same inversion pulses, but centered at -197 ppm instead of 197 ppm. The whole XTC measurement was repeated three times, and the three images were summed to improve image SNR. The parameter of gas-exchange function, f_D, defined as the fractional depolarization of gas-phase HPXe caused by the repeated RF inversion of dissolved-phase HPXe during continuous diffusive exchange of xenon between the two compartments, was calculated according to the ratio of the signal intensities of control and XTC images as follows:

$$f_D(\%) = \left(1 - \sqrt[N]{\frac{S_{XTC}}{S_{control}}}\right) \times 100 \quad [2]$$

where S_{XTC} and $S_{control}$ are the signal intensities of XTC and control images,

respectively, and N is the number of inversion pulses. f_D values were calculated on a pixel-by-pixel basis in order to create a whole lung f_D map. As with the r_a analysis, mean f_D values were obtained for each of the sham-instilled, CS and LPS, and EP-treated groups.

For each of the above described techniques, the existence of statistically-significant differences in mean values of derived parameters between groups was assessed by the analysis of variance (ANOVA) method with the Tukey-Kramer test, using the JMP Statistics package (SAS Institute Inc., Cary, NC, USA).

Histological Analysis

After completion of the MR experiments (week 10), the mice were euthanized with a lethal dose of carbon dioxide gas. Lungs were extracted and fixed in a 10 % formalin solution, and hematoxylin and eosin (H&E) stained slides were created to analyze morphological changes to the alveoli and terminal bronchioles. Four slides per mouse were used to evaluate structural parameters including mean linear intercept (MLI) and mean bronchial wall thickness (h), as previously described (31). Five MLI and h values were calculated from each slide, corresponding to the five lobar regions of the lung (right upper lobe, right middle lobe and right lower lobe; left upper lobe and left lower lobe). Each set of five values was averaged over the four slides, and then the resulting five averaged regional MLI and h values were in turn averaged to yield a single MLI and h value for each mouse. Mean MLI and h values were calculated for each of the sham-instilled, CS and LPS, and EP-treated groups in this manner.

In order to monitor morphological changes during the 10 weeks of CS and LPS administration, one additional CS and LPS histological analysis group (N=3 mice) was

prepared after 4 weeks of administration using the same protocol as described above. MLI and h values were evaluated for these groups as described above.

RESULTS

Figures 1 and 2 show the longitudinal changes in r_a and f_D maps, respectively, after 0, 6, 8 and 10 weeks of CS and LPS administration, for one representative mouse from each of the sham-instilled, CS and LPS, and EP-treated groups. It should be noted that Figures 1 and 2 were additionally processed with a 2 x 2 median filter using ImageJ (National Institute of Health) to reduce the prevalence of artifacts associated with cardiac motion and rapid diffusion of HPXe in the major airways. These maps depict the regional variation in pulmonary ventilation and gas-exchange functional changes over time. In particular, they highlight an approximately spatially homogeneous reduction of r_a in the CS and LPS mice after 10 weeks, and an overall improvement in r_a and f_D in response to EP therapy, with some regional heterogeneity.

Figures 3 and 4 display the group-mean values of r_a and f_D, respectively, after 0, 2, 6, 8 and 10 weeks of CS and LPS exposure. The mean r_a value for the CS and LPS group was found to be significantly decreased compared to that of the sham-instilled group after 6 weeks ($P < 0.05$), and was observed to continue to decrease for the remainder of the 10 week measurement period (after 10 weeks, $r_{a,CS\&LPS} = 0.19 \pm 0.03$, compared with $r_{a,Sham\text{-}instilled} = 0.25 \pm 0.03$, $P < 0.01$). The mean r_a value of the EP group was comparable to that of the sham-instilled mice ($r_{a,EP} = 0.25 \pm 0.03$) after 10 weeks, i.e. 4 weeks of EP administration. This value is also significantly larger than that of the CS and LPS group; $P < 0.01$. The f_D value of the CS and LPS group ($f_{D,CS\&LPS} = 4.5 \pm 1.1$ %) was significantly lower ($P < 0.01$) than that of the sham-instilled group ($f_{D,Sham\text{-}instilled} = 6.8 \pm 0.6$ %) after 10 weeks of exposure to CS

and LPS, while the f_D value of the EP group was considerably improved ($f_{D,EP}$ = 6.2 ± 0.9 %) compared with that of the CS and LPS group (P < 0.01). The longitudinal variation in mean r_a and f_D values from all groups was found to correlate significantly (Pearson's r = 0.820, P < 0.01).

Figures 5 and 6 depict whole lung mean MLI and h values and representative histological images obtained from mice from each of the sham-instilled, EP-treated and CS and LPS groups at the end of the 10 week experimental protocol, and the histological analysis group, respectively. As illustrated in these figures, an enlargement of the alveolar airspace volume was observed at week 10 following bronchial wall thickening; this is discussed below. The mean MLI of the CS and LPS group ($MLI_{CS\&LPS}$ = 44.0 ± 3.8 μm) was significantly larger than that of the sham-instilled group ($MLI_{Sham\text{-}instilled}$ = 39.7 ± 1.8 μm, P < 0.05). The mean MLI of the EP-treated group (MLI_{EP} = 38.2 ± 2.4 μm) was smaller than that of the CS and LPS group (P < 0.01) and similar to that of the sham-instilled group. The h value of the EP-treated group (h_{EP} = 12.5 ± 1.1 μm) was smaller than that of the CS and LPS group ($h_{CS\&LPS}$ = 14.9 ± 1.3 μm, P < 0.01), and similar to that of the sham-instilled group ($h_{Sham\text{-}instilled}$ = 12.3 ± 0.6 μm) at week 10. Meanwhile, the mean MLI and h values of the histological analysis group (exposed to CS and LPS for 4 weeks) were MLI_{HA_4w} = 39.8 ± 2.5 μm and h_{HA_4w} = 14.1 ± 0.6 μm, respectively, which were comparable to those of the sham-instilled mice.

Figure 7 shows correlation plots of individual r_a, f_D, h and MLI values obtained from the sham-instilled, EP-treated and CS and LPS mice after the 10 week experimental protocol. Significant positive correlations were observed between r_a and f_D,, and MLI and h, as were significant negative correlations between r_a and h, f_D and h, and f_D and MLI (P < 0.05). The correlation between r_a and MLI was not statistically

significant ($P > 0.05$).

DISCUSSION

In the present study, a murine model of COPD was developed by 10 weeks of exposure to CS and LPS, and the associated induced temporal changes of pulmonary ventilation and gas-exchange function were assessed noninvasively by HPXe MRI. The present COPD model was able to induce characteristic emphysematous alveolar tissue destruction, achieved by modifying previous protocols for producing airway inflammation using CS and LPS (21,32,33). The longitudinal HPXe MRI assessment of pulmonary function revealed a significant decrease in parameters of both fractional ventilation, r_a, and gas-exchange, f_D, of the CS and LPS mice after 6 weeks of CS and LPS exposure. However, for the first 2 weeks, pulmonary function in these mice was not notably different from that of sham-instilled mice. The longitudinal variation in the mean values of the two parameters was found to correlate, suggesting that the time-course of disease progression acted to simultaneously impair both ventilation and gas-exchange function. In addition, the r_a and f_D values were found to correlate significantly on a per mouse basis at week 10, although not prior to week 10, which supports the decision to end the CS and LPS administration at this time-point. Reductions in f_D and increases in the prevalence of ventilation defects have been previously observed using hyperpolarized gas MRI in human COPD patients (34,35), supporting the fact that the CS and LPS model of COPD employed here could successfully induce similar pathological effects to COPD itself. Combining whole-body CS exposure with LPS administration induced significant emphysematous pathology and bronchial wall thickening after 10 weeks of exposure, as illustrated by histology slides (Figures 5 and 6). On the other hand, exposure to only CS has been

reported to typically require ≥ 6 months to establish the characteristic emphysematous pathology in mice (36). While Hansbro et al. succeeded to establish a mouse model of COPD by 8 weeks of CS exposure through the nose only, this procedure required purpose-built equipment that is not readily translatable to our laboratory, and the CS dose was relatively high (2 cigarettes/mouse/day) (37). Thus, our protocol of CS and LPS exposure considerably shortened the time required to produce the two phenotypes of COPD pathology without necessitating specialist equipment. As such, this procedure may be advantageous for future investigations of COPD treatment response.

The present COPD mouse model caused significant decreases of ventilation and gas-exchange parameters: mean r_a of 0.19 ± 0.03 in CS and LPS mice compared with 0.25 ± 0.03 in sham-instilled mice; mean f_D of 4.5 ± 1.0% compared with 6.8 ± 0.6%, respectively, after 10 weeks. The decrease of r_a after 10 weeks of exposure to CS and LPS is indicative of an increase in the bronchial wall thickness, and indeed r_a showed a significant correlation with the histology-derived h value at this time-point (Figure 7). However, the decrease of f_D is indicative of both a reduction in the volume of septal tissue and an increase in the bronchial wall thickness. The decrease in f_D and r_a at the 6 week time-point may be attributable to the increase in bronchial wall thickness, h, (see Supporting Figure S1) since it is unlikely that the volume of septal tissue decreased (as there was no significant change in MLI at the 4 week time-point). This situation may be similar to a previous study in which CS and LPS were administered to rats for 6 weeks (21). According to that report, no histological evidence of COPD (i.e. MLI change) was seen despite overexpression of HMGB1. However, it is worth noting that these observations might not exclude the possibility of early stage emphysema, because mice lack the anatomical characteristics (respiratory bronchioles) for expression of centrilobular emphysema (4). One might also expect that the decrease in

f_D was caused in part by a reduction in the volume of the pulmonary capillaries, because the f_D measurement includes a contribution related to blood volume (since ddY-type mice exhibit only a single NMR peak from dissolved-phase ^{129}Xe in lung tissue and blood (31), and furthermore, the XTC technique as employed herein does not enable the distinction of two dissolved-phase ^{129}Xe compartments even if they were present).

In the present study, the efficacy of EP for treatment of the CS and LPS model of COPD was quantified by longitudinal observations of pulmonary function. The reductions in r_a and f_D in the CS and LPS group after 6 weeks recovered to a similar level as the sham-instilled group by 2 and 4 weeks of administration of EP, respectively ($P < 0.01$, see Figures 3 and 4). Because the administration of EP was only started 6 weeks after commencement of CS and LPS exposure (i.e. after some impairment of pulmonary function was observed), EP likely exhibited a combination of both preventative and therapeutic properties in the CS and LPS model of COPD. In other words, EP may have acted to inhibit further emphysema development and to repair the existing bronchial wall damage (Figures 5 and 6). This hypothesis is supported by the lack of significant difference in the r_a and f_D values between 6 and 10 week time-points in the EP-treated group ($P > 0.05$). However, the present study was unable to clarify whether the recovery of HPXe MRI metrics might be indicative of the reparation of tissue loss by early emphysema and/or improved pulmonary hemodynamics. To prove whether EP can indeed act to reverse emphysematous tissue loss, further experiments are needed in which EP administration is started after 10 weeks of CS and LPS exposure.

To the best of our knowledge, this is the first evidence of the therapeutic action of EP in a murine COPD model, as measured by HPXe MRI. Recently, it has been

reported that intraperitoneal administration of EP can inhibit the expression of HMGB1 (18,19). Additionally, high expression of HMGB1 has been reported to lead to lung functional impairment, and is associated with the development and progression of COPD (20-22). On the other hand, albeit paradoxically, the HMGB1/RAGE pathway is also known to be associated with a series of signalling pathways for tissue repair (23,24). It may be speculated that EP is effective in treating lung diseases caused by chronic inflammation (such as the CS and LPS model of COPD) through the regulation of HMGB1/RAGE, leading to improvement and potentially maintenance of murine pulmonary function. Further studies with corresponding molecular assays are required to substantiate this claim.

CONCLUSION

The feasibility of HPXe MRI for longitudinal assessment of disease progression and pharmacological therapy has been demonstrated in a mouse model of COPD. The model, combining exposure to cigarette smoke and lipopolysaccharide solution, induced COPD characteristics in mice in a relatively short time of 10 weeks and offers potential advantages for pharmacological therapy assessment applications. HPXe MRI-derived metrics of pulmonary function showed considerable impairment in both ventilation and gas-exchange function in CS and LPS mice compared with sham-instilled mice, as verified by histological analysis. Longitudinal HPXe MRI assessment of the action of an anti-inflammatory agent, ethyl pyruvate, for treatment of this COPD model revealed preliminary evidence of its efficacy, and may help to elucidate the exact mechanisms of its therapeutic action in the future.

Acknowledgements

This work was supported by the Japan Society for the Promotion of Science (JSPS) KAKENHI grant numbers: JP24300163 and JP15H03006. NJS acknowledges funding support from the Medical Research Council (MRC) and the JSPS summer programme (2015).

References

1. Lozano R, Naghavi M, Foreman K, et al. Global and regional mortality from 235 causes of death for 20 age groups in 1990 and 2010: a systematic analysis for the Global Burden of Disease Study 2010. The Lancet 2012;380(9859):2095-2128.
2. Holgate S, Agusti A, Strieter RM, Anderson GP, Fogel R, Bel E, Martin TR, Reiss TF. Drug development for airway diseases: looking forward. Nat Rev Drug Discov 2015;14:367-368.
3. Fricker M, Deane A, Hansbro PM. Animal models of chronic obstructive pulmonary disease. Expert Opin Drug Discov 2014;9(6):629-645.
4. Gardi C, Stringa B, Martorana PA. Animal models for anti-emphysema drug discovery. Expert Opin Drug Discov 2015;10(4):399-410.
5. Mizutani N, Fuchikami J, Takahashi M, Nabe T, Yoshino S, Kohno S. Pulmonary emphysema induced by cigarette smoke solution and lipopolysaccharide in guinea pigs. Biol Pharm Bull 2009;32:1559-1564.
6. Li JJ, Wang W, Baines KJ, Bowden NA, Hansbro PM, Gibson PG, Kumar RK, Foster PS, Yang M. IL-27/IFN-γ induce MyD88-dependent steroid-resistant airway hyperresponsiveness by inhibiting glucocorticoid signaling in macrophages. J Immunol 2010;185(7):4401-4409.
7. Fain SB, Korosec FR, Holmes JH, O'Halloran R, Sorkness RL, Grist TM. Functional lung imaging using hyperpolarized gas MRI. J Magn Reson Imag 2007;25(5):910-923.
8. Mugler JP, III, Altes TA. Hyperpolarized ^{129}Xe MRI of the human lung. J Magn Reson Imag 2013;37(2):313-331.
9. van Beek EJR, Wild JM, Kauczor H-U, Schreiber W, Mugler JP, de Lange EE. Functional MRI of the lung using hyperpolarized 3-helium gas. J Magn Reson Imag

2004;20(4):540-554.

10. Kirby M, Pike D, Coxson HO, McCormack DG, Parraga G. Hyperpolarized ^{3}He ventilation defects used to predict pulmonary exacerbations in mild to moderate chronic obstructive pulmonary disease. Radiology 2014;273(3):887-896.
11. Qing K, Mugler JP 3rd, Altes TA, Jiang Y, Mata JF, Miller GW, Ruset IC, Hersman FW, Ruppert K. Assessment of lung function in asthma and COPD using hyperpolarized ^{129}Xe chemical shift saturation recovery spectroscopy and dissolved-phase MRI. NMR Biomed 2014;27(12):1490-1501.
12. Imai H, Kimura A, Fujiwara H. Small animal imaging with hyperpolarized ^{129}Xe magnetic resonance. Anal Sci 2014;30(1):157-166.
13. Tetsumoto S, Takeda Y, Imai H, et al. Validation of noninvasive morphological and diffusion imaging in mouse emphysema by micro-computed tomography and hyperpolarized ^{129}Xe magnetic resonance imaging. Am J Respir Cell Mol Biol 2013;49(4):592-600.
14. Kung CW, Lee YM, Cheng PY, Peng YJ, Yen MH. Ethyl pyruvate reduces acute lung injury via regulation of iNOS and HO-1 expression in endotoxemic rats. J Surg Res 2011;167(2):e323-e331.
15. Liu C, Fang C, Cao G, Liu K, Wang B, Wan Z, Li S, Wu S. Ethyl pyruvate ameliorates monocrotaline-induced pulmonary arterial hypertension in rats. J Cardiovasc Pharmacol 2014;64(1):7-15.
16. Shang GH, Lin DJ, Xiao W, Jia CQ, Li Y, Wang AH, Dong L. Ethyl pyruvate reduces mortality in an endotoxin-induced severe acute lung injury mouse model. Respir Res 2009;10:91.
17. Pulathan Z, Altun G, Hemşinli D, Menteşe A, Yuluğ E, Civelek A. Role of ethyl pyruvate in systemic inflammatory response and lung injury in an experimental

model of ruptured abdominal aortic aneurysm. Biomed Res Int 2014;2014:857109.

18. Cheng P, Dai W, Wang F, Lu J, Shen M, Chen K, Li J, Zhang Y, Wang C, Yang J, Zhu R, Zhang H, Zheng Y, Guo C-Y, Xu L. Ethyl pyruvate inhibits proliferation and induces apoptosis of hepatocellular carcinoma via regulation of the HMGB1–RAGE and AKT pathways. Biochem Biophys Res Commun 2014;443(4):1162-1168.
19. Lee YM, Kim J, Jo K, Shin SD, Kim C-S, Sohn EJ, Kim SG, Kim JS. Ethyl Pyruvate Inhibits Retinal Pathogenic Neovascularization by Downregulating HMGB1 Expression. J Diabetes Res 2013;2013:8.
20. Ko H-K, Hsu W-H, Hsieh C-C, Lien T-C, Lee T-S, Kou YR. High expression of high-mobility group box 1 in the blood and lungs is associated with the development of chronic obstructive pulmonary disease in smokers. Respirology 2014;19(2):253-261.
21. Wang CM, Jiang M, Wang HJ. Effect of NF-κB inhibitor on high-mobility group protein B1 expression in a COPD rat model. Mol Med Rep 2013;7(2):499-502.
22. Zhang Y, Li S, Wang G, Han D, Xie X, Wu Y, Xu J, Lu J, Li F, Li M. Changes of HMGB1 and sRAGE during the recovery of COPD exacerbation. J Thorac Dis 2014;6(6):734-741.
23. Lee DE, Trowbridge RM, Ayoub NT, Agrawal DK. High-mobility Group Box Protein-1, Matrix Metalloproteinases, and Vitamin D in Keloids and Hypertrophic Scars. Plast Reconstr Surg Glob Open 2015;3(6):e425.
24. Pandolfi F, Altamura S, Frosali S, Conti P. Key Role of DAMP in Inflammation, Cancer, and Tissue Repair. Clin Ther 2016;38(5):1017-1028.
25. Walker TG, Happer W. Spin-exchange optical pumping of noble-gas nuclei. Reviews of Modern Physics 1997;69(2):629-642.
26. Imai H, Fukutomi J, Kimura A, Fujiwara H. Effect of reduced pressure on the

polarization of ^{129}Xe in the production of hyperpolarized ^{129}Xe gas: Development of a simple continuous flow mode hyperpolarizing system working at pressures as low as 0.15 atm. Concepts in Magnetic Resonance Part B: Magnetic Resonance Engineering 2008;33B(3):192-200.

27. Imai H, Kimura A, Hori Y, Iguchi S, Kitao T, Okubo E, Ito T, Matsuzaki T, Fujiwara H. Hyperpolarized ^{129}Xe lung MRI in spontaneously breathing mice with respiratory gated fast imaging and its application to pulmonary functional imaging. NMR Biomed 2011;24:1343-1352.
28. Imai H, Matsumoto H, Miyakoshi E, Okumura S, Fujiwara H, Kimura A. Regional fractional ventilation mapping in spontaneously breathing mice using hyperpolarized ^{129}Xe MRI. NMR Biomed 2015;28:24-29.
29. Hamedani H, Clapp JT, Kadlecek SJ, Emami K, Ishii M, Gefter WB, Xin Y, Cereda M, Shaghaghi H, Siddiqui S, Rossman MD, Rizi RR. Regional Fractional Ventilation by Using Multibreath Wash-in ^{3}He MR Imaging. Radiology 2016;279(3):917-924.
30. Ruppert K, Brookeman JR, Hagspiel KD, Mugler JP, III. Probing lung physiology with xenon polarization transfer contrast (XTC). Magn Reson Med 2000;44(3):349-357.
31. Imai H, Kimura A, Iguchi S, Hori Y, Masuda S, Fujiwara H. Non-invasive Detection of Pulmonary Tissue Destruction in a Mouse Model of Emphysema Using Hyperpolarized ^{129}Xe MRS under Spontaneous Respiration. Magn Reson Med 2010;64(4):929-938.
32. Hardaker EL, Freeman MS, Dale N, Bahra P, Raza F, Banner KH, Poll C. Exposing rodents to a combination of tobacco smoke and lipopolysaccharide results in an exaggerated inflammatory response in the lung. Br J Pharmacol

2010;160(8):1985-1996.

33. Song HH, Shin IS, Woo SY, Lee SU, Sung MH, Ryu HW, Kim DY, Ahn KS, Lee HK, Lee D, Oh SR. Piscroside C, a novel iridoid glycoside isolated from Pseudolysimachion rotundum var. subinegrum suppresses airway inflammation induced by cigarette smoke. J Ethnopharmacol 2015;170:20-27.
34. Dregely I, Mugler JP, III, Ruset IC, Altes TA, Mata JF, Miller GW, Ketel J, Ketel S, Distelbrink J, Hersman FW, Ruppert K. Hyperpolarized Xenon-129 gas-exchange imaging of lung microstructure: first case studies in subjects with obstructive lung disease. J Masgn Reson Imag 2011;33(5):1052-1062.
35. Kirby M, Svenningsen S, Owrangi A, Wheatley A, Farag A, Ouriadov A, Santyr GE, Etemad-Rezai R, Coxson HO, McCormack DG, Parraga G. Hyperpolarized ^{3}He and ^{129}Xe MR Imaging in Healthy Volunteers and Patients with Chronic Obstructive Pulmonary Disease. Radiology 2012;265(2):600-610.
36. Churg A, Cosio M, Wright JL. Mechanisms of cigarette smoke-induced COPD: insights from animal models. Am J Physiol Lung Cell Mol Physiol 2008;294(4):L612-631.
37. Beckett EL, Stevens RL, Jarnicki AG, et al. A new short-term mouse model of chronic obstructive pulmonary disease identifies a role for mast cell tryptase in pathogenesis. J Allergy Clin Immunol 2013;131(3):752-762.

Figure legends:

Figure 1. Example parametric maps of r_a derived from longitudinal studies of mice in each of the three groups, from top to bottom: sham-instilled; CS and LPS model of COPD; EP-treated. In all cases, the time course is shown horizontally.

Figure 2. Example parametric maps of f_D derived from longitudinal studies of mice in each of the three groups, from top to bottom: sham-instilled; CS and LPS model of COPD; EP-treated. In all cases, the time course is shown horizontally.

Figure 3. Box plots of the temporal change of mean r_a values for all mice, separated by group. Significant differences between groups are indicated by solid lines, along with the corresponding p values of significance (*$P < 0.05$; ** $P < 0.01$).

Figure 4. Box plots of the temporal change of mean f_D values for all mice, separated by group. Significant differences between groups are indicated by solid lines, along with the corresponding p values of significance (*$P < 0.05$; ** $P < 0.01$).

Figure 5. a) Box plots showing the mean MLI values obtained from mice in each of the four groups, from left to right: sham-instilled; histological analysis (CS&LPS 4w), CS and LPS model of COPD (CS&LPS10w); EP-treated. b) Representative examples of

H&E stained histology slides obtained from 5 lung regions of one mouse chosen from each of the four groups. RU, right upper lobe; RM, right middle lobe; RL, right lower lobe; LU, upper region of the left lobe; LL, lower region of the left lobe. Note: mean values in a) represent the mean of the whole group; mean values in b) represent the mean for the selected mouse from each group.

Figure 6. a) Box plots showing the mean bronchial wall thickness (h) values obtained from mice in each of the four groups, from left to right: sham-instilled; histological analysis (CS&LPS 4w), CS and LPS model of COPD (CS&LPS10w); EP-treated after the 10 week experimental protocol. b) Representative examples of H&E stained histology slides obtained from the four groups.

Figure 7. Relationships between HPXe MRI-derived parameters of pulmonary function (r_a and f_D), and histology-derived parameters of lung structure (MLI and h) obtained from the sham-instilled (□), EP-treated (○), and CS and LPS (▲) mice after the 10 week experimental protocol. The Pearson's r value and P value of statistical significance are noted in each plot.

Supporting Figure S1. a) Box plots showing the mean bronchial wall thickness (h) values obtained from mice in each of the five groups, from left to right: sham-instilled; histological analysis (CS&LPS 4w and CS&LPS 6w), CS and LPS model of COPD (CS&LPS10w); EP-treated after the 10 week experimental protocol. b) Representative examples of H&E stained histology slides obtained from the five groups.

Treatment response of ethyl pyruvate in a mouse model of chronic obstructive pulmonary disease studied by hyperpolarized ^{129}Xe MRI

Atsuomi Kimura,*[1] Yukiko Yamauchi,[1] Shota Hodono,[1] Neil James Stewart,[2] Osamu Hosokawa,[1] Yu Hagiwara,[1] Hirohiko Imai,[3] and Hideaki Fujiwara[1]

[1] Department of Medical Physics and Engineering, Division of Medical Technology and Science, Faculty of Health Science, Graduate School of Medicine, Osaka University

[2] Academic Unit of Radiology, University of Sheffield, Sheffield, South Yorkshire, UK

[3] Research and Educational Unit of Leaders for Integrated Medical System, Center for the Promotion of Interdisciplinary Education and Research, Kyoto University, Kyoto, Japan

Running head:

HPXe MRI of murine COPD model and therapy response

Word count: 4492

*Corresponding author: Atsuomi Kimura, PhD, Department of Medical Physics and Engineering, Division of Medical Technology and Science, Faculty of Health Science, Graduate School of Medicine, Osaka University, 1-7 Yamadaoka, Suita, Osaka 565-0871, Japan,

Phone: +81-6-6879-2478, E-mail: kimura@sahs.med.osaka-u.ac.jp

ABSTRACT

Purpose: To investigate disease progression and treatment response in a murine model of chronic obstructive pulmonary disease (COPD) using a preclinical hyperpolarized ^{129}Xe (HPXe) MRI strategy.

Methods: COPD phenotypes were induced in 32 mice by 10 weeks of exposure to cigarette smoke (CS) and lipopolysaccharide (LPS). The efficacy of ethyl pyruvate (EP), an anti-inflammatory drug, was investigated by administering EP to 16 of the 32 mice after 6 weeks of CS and LPS exposure. HPXe MRI was performed to monitor changes in pulmonary function during disease progression and pharmacological therapy.

Results: HPXe metrics of fractional ventilation and gas-exchange function were significantly reduced after 6 weeks of CS and LPS exposure compared to sham-instilled mice administered with saline ($P < 0.05$). After this observation, EP administration was started in 16 of the 32 mice and continued for 4 weeks. EP was found to improve HPXe MRI metrics to a similar level as in sham-instilled mice ($P < 0.01$). Histological analysis showed significant alveolar tissue destruction in the COPD group, but relatively normal alveolar structure in the EP and sham-instilled groups.

Conclusion: This study demonstrates the potential efficacy of EP for COPD therapy, as assessed by a non-invasive, translatable ^{129}Xe MRI procedure.

Abstract word count: 200

Keywords: Hyperpolarized ^{129}Xe MRI, lung functional assessment, murine chronic obstructive pulmonary disease, treatment response, ethyl pyruvate

Comment [XH1]: R1.6

Comment [XH2]: R1.7

Comment [XH3]: R1.8

Comment [XH4]: R1.9

INTRODUCTION

Chronic obstructive pulmonary disease (COPD), a heterogeneous lung disease characterized by both chronic airway inflammation and emphysematous alveolar tissue destruction, is predicted to be the third leading cause of death worldwide by 2020 (1). At present, pharmacological therapies for COPD have shown limited efficacy and thus the development of new therapeutic drugs is vital for improving patient outcomes (2). The use of appropriate animal models of COPD that adequately induce the key symptoms of the disease is indispensable for therapy development, and rodent models are especially important. In particular, preclinical studies with mice are often appropriate because a wide range of well-characterized disease models are available (3,4). As smoking and repeated lung infections are the primary causes of COPD, several murine COPD models have been developed by exposing mice to cigarette smoke. Despite certain models showing good reproducibility for inducing the two main phenotypes of COPD mentioned above, the lack of applicable methods for assessment and diagnosis of these disease models remains a limiting factor for preclinical studies. Most previous studies have relied on plethysmography and/or histology to evaluate the applicability of murine COPD models, necessitating a tracheostomy and/or mouse death for each examination (5,6) and hence making it difficult to evaluate drug efficacy repetitively and longitudinally. To help resolve this problem, non-invasive imaging techniques that allow the longitudinal assessment of disease progression and therapeutic efficacy of drugs in vivo are required.

MRI using hyperpolarized (HP) noble gases (^{3}He and ^{129}Xe) as contrast agents offers an attractive means to visualize and quantitatively evaluate pulmonary functional parameters such as ventilation and gas-exchange (7-9). In a number of studies in small animals and humans, pathological changes of these fundamental

Comment [XH5]: R1.10

parameters have been investigated using HP gas MRI and quantitative measures of ventilation and gas-exchange dysfunction caused by COPD have been established (10,11). HP ^{129}Xe (HPXe) is a versatile contrast agent to evaluate drug efficacy in the lungs because it allows not only imaging of ventilation, but also the assessment of pulmonary gas-exchange, thanks to its solubility in pulmonary tissues and blood. To this end, we have developed a continuous-flow mode polarizer for HPXe production and have established non-invasive MRI procedures under spontaneous respiration for the assessment of pulmonary function in mice (12,13). In this study, we apply our HPXe methodology to explore the feasibility of a new drug for COPD therapy.

Comment [XH6]: R1.15

Ethyl pyruvate (EP), an anti-inflammatory agent, is a candidate for pharmacological therapy of COPD. In recent years, EP has been shown to demonstrate therapeutic efficacy in various animal models of lung diseases, such as acute lung injury (ALI) and pulmonary arterial hypertension (PAH) (15-17). The therapeutic efficacy of EP is attributed to its ability to regulate high-mobility group box protein-1 (HMGB1) release from innate immune cells, and to deactivate subsequent cytokine production that would further stimulate inflammatory responses (18,19). HMGB1, which is an abundant chromatin protein, may play a crucial role in pharmacological therapy of COPD because it is known to not only trigger inflammatory responses but also, paradoxically, to activate cells involved in tissue repair (20-24). HMGB1 functions by binding with the receptor for advanced glycation end products (RAGE) and Toll-Like Receptors 2 and 4. In recent years, it has been shown that HMGB1 can also initiate wound healing processes through binding with RAGE followed by activation of the extracellular signal-regulated kinase 1/2 (ERK1/2) signaling pathway (23). RAGE is expressed in pulmonary tissues with relatively high basal levels (22), and EP has been reported to activate the ERK1/2 signaling pathway (14). Thus, EP

shows considerable potential as a drug for lung tissue repair accompanied with anti-inflammatory responses through regulation of the HMGB1/RAGE pathway.

Comment [XH7]: R2.1

In the present study, we demonstrate the observation of disease progression in a mouse model of COPD induced by cigarette smoke (CS) exposure and lipopolysaccharide (LPS) instillation, as measured by HPXe MRI. Additionally, the efficacy of ethyl pyruvate (EP) for treatment of this COPD model is studied to assess the feasibility of this non-invasive imaging technique as a diagnostic method for early disease detection and therapy response evaluation in COPD.

METHODS

Animal preparation

Thirty-seven male, 6-week-old, type ddY mice, weighing 30 – 35 g (Japan SLC, Inc., Shizuoka, Japan) were included in this study. All experimental procedures and animal care standards conformed to Osaka University guidelines. Mice were divided into two groups: a sham-instilled group of N=5 mice and a CS and LPS group of N=32. The CS and LPS mice were further divided into 2 equal groups of 16 individuals. The two subgroups were separately administered with a combination of CS and LPS as follows. CS of approximately 2.1 L in volume resulting from one cigarette (Lark Milds: tar 9 mg, nicotine 0.8 mg; Philip Morris International Inc., New York, USA) was collected into a Tedlar® bag (Sigma-Aldrich, St Louis, MO, USA). The mice in each subgroup were placed in a semi-sealed plastic container with a volume of 12.4 L and 9 airshafts of 5 mm inner diameter on its upper surface. CS was flowed from the Tedlar® bag into the container for 26 minutes at a rate of 40 mL/min. Following this, fresh room air was flowed into the container for 5 minutes (at 720 mL/min). This whole-body exposure

procedure was performed twice daily on five consecutive days within one week, and repeated on a weekly basis as described below. On each fifth day, a 20 µL solution of LPS in saline (0.4 mg/kg, LPS in *Escherichia coli*, serotype O55:B5, Sigma-Aldrich, St. Louis, MO, USA) was delivered intra-tracheally to the mice at least 2 hours prior to the CS exposure. The sham-instilled mice were intra-tracheally administered with 20 µL of saline on every fifth day in the same manner as the LPS administration.

Six weeks after commencing CS and LPS exposure, the two subgroups of CS and LPS mice were assigned as follows: a pure CS and LPS group of N=16 mice and an EP-treated group of N=16 mice. For the pure CS and LPS group, the same protocol of CS and LPS administration was continued for a further 4 weeks. EP-treated mice were intra-tracheally administered with a 20 µL solution of EP in saline (1.3 mg/kg, Tokyo Chemical Industry Ltd, Tokyo, Japan) on a daily basis for 4 weeks, in addition to the continued administration of CS and LPS as detailed above. EP was always administered after the CS and LPS exposure, separated by an interval of at least 2 hours. Therefore, in total, 10 weeks were required to completely prepare the CS and LPS, and EP-treated groups. The sham-instilled mice were intra-tracheally administered with 20 µL of saline per day, every weekday, for this 4 week period, in the same manner as the EP treatment. The survival rates of the whole 10-week procedure were 75% for CS and LPS mice (12 out of 16 mice survived), 75% for EP-treated mice (12 out of 16 mice survived), and 100 % for the sham-instilled group.

In all cases, prior to the instillation of saline, LPS or EP solution, mice were anesthetized with 2% isoflurane (ISOFLU®, Dainippon Sumitomo Pharmaceutical Co. Ltd, Osaka, Japan), which was administered via a nose cone using a home-built anesthesia system connected to an isoflurane vaporizer (Isorex I-200, Shin-Ei

Industries, Inc., Tokyo, Japan). Subsequently, mice were intubated with a 22 G catheter (SURFLO® F&F, Terumo Corp., Tokyo, Japan) while positioned supine and secured to a slanted wooden board, and then the saline, LPS or EP solution was instilled.

MR measurements of sham-instilled and CS and LPS groups were performed at 0 weeks (prior to the first administration) and 2, 6, 8 and 10 weeks after commencing the administration of CS and LPS. Similarly, MR measurements of the EP-treated group were performed at 0, 6, 8 and 10 weeks after commencing the administration of CS and LPS (i.e. -6, 0, 2 and 4 weeks from commencement of EP therapy). Immediately before all MR measurements, mice were anesthetized with 2 % isoflurane as detailed above. A plastic mouth mask, to which three polyethylene tubes were connected (for HPXe gas delivery, O_2 delivery and exhaled gas exhaust), was attached to the animal prior to placement in the MR scanner. In order to synchronize image acquisitions with respiratory motion, a pulse transducer (AD Instruments Ltd., Dunedin, New Zealand) was positioned on the mouse abdomen, just inferior to the diaphragm. This sensor converted the respiratory motion into an electrical signal that was monitored in real-time using LabVIEW software (National Instruments, Austin, TX, USA). The animal's body temperature in the magnet was maintained with warm water circulating through a rubber tube placed on the abdomen. The MR imaging procedure was performed without tracheal intubation or tracheotomy and hence was entirely non-invasive.

^{129}Xe Polarization and Gas Delivery

^{129}Xe nuclei were polarized to ~10% by Rb-^{129}Xe spin-exchange optical pumping (25) with a home-built continuous-flow ^{129}Xe polarizer (26). A gas mixture consisting of 70% Xe (natural abundance, comprising 26% ^{129}Xe) and 30% N_2 was supplied from a pre-mixed cylinder (Air Liquid Japan Ltd., Tokyo, Japan) at a pressure of 0.15 atmospheres for ^{129}Xe polarization. Once polarized, HPXe was subsequently compressed to atmospheric pressure with a diaphragm pump (LABOPORT® N86 KN.18, KNF Neuberger GmbH, Freiburg, Germany) to facilitate gas delivery directly and continuously from the polarizing cell to the mouse in the magnet. The HPXe gas mixture was flowed continuously at a rate of 50 mL/min to each mouse and was mixed with O_2 (continuously supplied at 9 mL/min) in the mouth mask. The percentages of Xe and O_2 spontaneously inhaled by the mice were 59.3% and 15.3%, respectively.

MR Imaging

All MR measurements were performed on a Varian Unity INOVA 400 WB high-resolution NMR spectrometer system running VNMR 6.1C software (Varian Inc., Palo Alto, CA, USA). A 9.4 T vertical magnet with a bore width of 89 mm (Oxford Instruments Plc., Oxford, UK) was used. A self-shielded gradient probe was employed in combination with Litz volume RF coils of 34 mm inner diameter, tunable to the Larmor frequencies of ^{129}Xe (110.6 MHz) and ^{1}H (399.6 MHz) (Clear Bore DSI-1117, Doty Scientific, Inc., Columbia, SC, USA).

For assessment of pulmonary ventilation and gas-exchange function, HPXe gas images were acquired with a 2D multi-shot balanced steady-state free precession (bSSFP) sequence, which was programmed in-house (27). Acquisition parameters were as follows: RF pulse, 1000 μs long Gaussian-shaped pulse with a bandwidth of 2800 Hz and centered on the ^{129}Xe gas-phase resonance (0 ppm); TR/TE, 3.2/1.6 ms;

receiver bandwidth, 62 kHz; one coronal slice of thickness 20 mm, covering the whole of the lungs; matrix size, 64 × 32; field of view, 80 × 25.6 mm^2; number of shots (required to fill k-space), 4; flip angle, 40°; number of averages of the whole acquisition, 8; centrically-ordered phase encoding. ^{129}Xe images were reconstructed by a 2D fast Fourier transform after zero filling to a 128 × 64 matrix using in-house MATLAB scripts (MathWorks Inc., Natick, MA, USA).

Comment [XH8]: R1.16

Evaluation of ventilation function

For evaluating pulmonary ventilation function, the fractional ventilation (i.e. the fraction of gas "turned over" per breathing cycle), r_a, was mapped across the lungs following a previously reported method (28,29). Briefly, after the HPXe concentration in the lungs had reached a steady-state under the continuous supply of HPXe and O_2, two pre-saturation RF pulses were applied at the ^{129}Xe gas-phase frequency to destroy any gas-phase ^{129}Xe magnetization in the alveoli. The bSSFP imaging sequence was then used to acquire respiratory-synchronized ^{129}Xe gas ventilation images at inspiration after n breathing cycles. The value of n was sequentially incremented from 1 to 10, and then to 12, 15 and 20; thus, thirteen ^{129}Xe ventilation images were acquired in total. (In Reference (28), images were acquired after 1 to 10 breaths only; the purpose of the additional acquired images here was to improve the accuracy of the r_a estimate.) From the resulting image series, the fractional ventilation of each voxel was evaluated by analyzing the dependency of the ^{129}Xe MR signal intensity upon the number of breaths (Equations 2 and 3, Reference (28)). The fractional ventilation, r_a, is defined as:

Comment [XH9]: R1.18

Comment [XH10]: R1.19

$$r_a = \frac{V_f}{V_o + V_f}, \qquad [1]$$

where V_o and V_f denote the volumes of old and new (fresh) gas within the voxel after each breath, respectively. r_a values were determined pixel-by-pixel over the whole image to derive a r_a map, and averaged for each mouse to obtain the whole lung r_a. Finally, the whole lung r_a values were averaged for each of the sham-instilled, CS and LPS, and EP-treated groups to obtain group mean r_a values.

Evaluation of gas-exchange function

The efficiency of HPXe gas-exchange between the alveoli (gas-phase) and the lung parenchyma and capillaries (dissolved-phase) was evaluated by the xenon polarization transfer contrast (XTC) method (30). Briefly, a XTC image was generated by acquiring bSSFP gas ventilation images at expiration, separated by the application of four frequency-selective inversion pulses (inter-pulse delay 20 ms) at the Larmor frequency of dissolved-phase ^{129}Xe (197 ppm), and comparing the resulting ventilation image intensities (27). The flip angle of the inversion pulse (Gaussian-shape; 1000 μs duration) was calibrated prior to the present study. Similarly, a "control" bSSFP image was generated by acquiring ventilation images at expiration, separated by the application of the same inversion pulses, but centered at -197 ppm instead of 197 ppm. The whole XTC measurement was repeated three times, and the three images were summed to improve image SNR. The parameter of gas-exchange function, f_D, defined as the fractional depolarization of gas-phase HPXe caused by the repeated RF inversion of dissolved-phase HPXe during continuous diffusive exchange of xenon between the two compartments, was calculated according to the ratio of the signal intensities of control and XTC images as follows:

$$f_D(\%) = \left(1 - \sqrt[N]{\frac{S_{XTC}}{S_{control}}}\right) \times 100 \quad [2]$$

where S_{XTC} and $S_{control}$ are the signal intensities of XTC and control images,

Comment [XH11]: R1.1

Comment [XH12]: R1.20

Comment [XH13]: R1.1

respectively, and N is the number of inversion pulses. f_D values were calculated on a pixel-by-pixel basis in order to create a whole lung f_D map. As with the r_a analysis, mean f_D values were obtained for each of the sham-instilled, CS and LPS, and EP-treated groups.

For each of the above described techniques, the existence of statistically-significant differences in mean values of derived parameters between groups was assessed by the analysis of variance (ANOVA) method with the Tukey-Kramer test, using the JMP Statistics package (SAS Institute Inc., Cary, NC, USA).

Histological Analysis

After completion of the MR experiments (week 10), the mice were euthanized with a lethal dose of carbon dioxide gas. Lungs were extracted and fixed in a 10 % formalin solution, and hematoxylin and eosin (H&E) stained slides were created to analyze morphological changes to the alveoli and terminal bronchioles. Four slides per mouse were used to evaluate structural parameters including mean linear intercept (MLI) and mean bronchial wall thickness (h), as previously described (31). Five MLI and h values were calculated from each slide, corresponding to the five lobar regions of the lung (right upper lobe, right middle lobe and right lower lobe; left upper lobe and left lower lobe). Each set of five values was averaged over the four slides, and then the resulting five averaged regional MLI and h values were in turn averaged to yield a single MLI and h value for each mouse. Mean MLI and h values were calculated for each of the sham-instilled, CS and LPS, and EP-treated groups in this manner.

Comment [XH14]: R1.21&22

In order to monitor morphological changes during the 10 weeks of CS and LPS administration, one additional CS and LPS histological analysis group (N=3 mice) was

prepared after 4 weeks of administration using the same protocol as described above. MLI and h values were evaluated for these groups as described above.

RESULTS

Figures 1 and 2 show the longitudinal changes in r_a and f_D maps, respectively, after 0, 6, 8 and 10 weeks of CS and LPS administration, for one representative mouse from each of the sham-instilled, CS and LPS, and EP-treated groups. It should be noted that Figures 1 and 2 were additionally processed with a 2 x 2 median filter using ImageJ (National Institute of Health) to reduce the prevalence of artifacts associated with cardiac motion and rapid diffusion of HPXe in the major airways. These maps depict the regional variation in pulmonary ventilation and gas-exchange functional changes over time. In particular, they highlight an approximately spatially homogeneous reduction of r_a in the CS and LPS mice after 10 weeks, and an overall improvement in r_a and f_D in response to EP therapy, with some regional heterogeneity.

Comment [XH15]: R1.2

Figures 3 and 4 display the group-mean values of r_a and f_D, respectively, after 0, 2, 6, 8 and 10 weeks of CS and LPS exposure. The mean r_a value for the CS and LPS group was found to be significantly decreased compared to that of the sham-instilled group after 6 weeks ($P < 0.05$), and was observed to continue to decrease for the remainder of the 10 week measurement period (after 10 weeks, $r_{a,CS\&LPS} = 0.19 \pm 0.03$, compared with $r_{a,Sham\text{-}instilled} = 0.25 \pm 0.03$, $P < 0.01$). The mean r_a value of the EP group was comparable to that of the sham-instilled mice ($r_{a,EP} = 0.25 \pm 0.03$) after 10 weeks, i.e. 4 weeks of EP administration. This value is also significantly larger than that of the CS and LPS group; $P < 0.01$. The f_D value of the CS and LPS group ($f_{D,CS\&LPS} = 4.5 \pm 1.1$ %) was significantly lower ($P < 0.01$) than that of the sham-instilled group ($f_{D,Sham\text{-}instilled} = 6.8 \pm 0.6$ %) after 10 weeks of exposure to CS

and LPS, while the f_D value of the EP group was considerably improved ($f_{D,EP}$ = 6.2 ± 0.9 %) compared with that of the CS and LPS group (P < 0.01). The longitudinal variation in mean r_a and f_D values from all groups was found to correlate significantly (Pearson's r = 0.820, P < 0.01).

Figures 5 and 6 depict whole lung mean MLI and h values and representative histological images obtained from mice from each of the sham-instilled, EP-treated and CS and LPS groups at the end of the 10 week experimental protocol, and the histological analysis group, respectively. As illustrated in these figures, an enlargement of the alveolar airspace volume was observed at week 10 following bronchial wall thickening; this is discussed below. The mean MLI of the CS and LPS group ($MLI_{CS\&LPS}$ = 44.0 ± 3.8 μm) was significantly larger than that of the sham-instilled group ($MLI_{Sham\text{-}instilled}$ = 39.7 ± 1.8 μm, P < 0.05). The mean MLI of the EP-treated group (MLI_{EP} = 38.2 ± 2.4 μm) was smaller than that of the CS and LPS group (P < 0.01) and similar to that of the sham-instilled group. The h value of the EP-treated group (h_{EP} = 12.5 ± 1.1 μm) was smaller than that of the CS and LPS group ($h_{CS\&LPS}$ = 14.9 ± 1.3 μm, P < 0.01), and similar to that of the sham-instilled group ($h_{Sham\text{-}instilled}$ = 12.3 ± 0.6 μm) at week 10. Meanwhile, the mean MLI and h values of the histological analysis group (exposed to CS and LPS for 4 weeks) were MLI_{HA_4w} = 39.8 ± 2.5 μm and h_{HA_4w} = 14.1 ± 0.6 μm, respectively, which were comparable to those of the sham-instilled mice.

Figure 7 shows correlation plots of individual r_a, f_D, h and MLI values obtained from the sham-instilled, EP-treated and CS and LPS mice after the 10 week experimental protocol. Significant positive correlations were observed between r_a and f_D, and MLI and h, as were significant negative correlations between r_a and h, f_D and h, and f_D and MLI (P < 0.05). The correlation between r_a and MLI was not statistically

significant ($P > 0.05$).

DISCUSSION

In the present study, a murine model of COPD was developed by 10 weeks of exposure to CS and LPS, and the associated induced temporal changes of pulmonary ventilation and gas-exchange function were assessed noninvasively by HPXe MRI. The present COPD model was able to induce characteristic emphysematous alveolar tissue destruction, achieved by modifying previous protocols for producing airway inflammation using CS and LPS (21,32,33). The longitudinal HPXe MRI assessment of pulmonary function revealed a significant decrease in parameters of both fractional ventilation, r_a, and gas-exchange, f_D, of the CS and LPS mice after 6 weeks of CS and LPS exposure. However, for the first 2 weeks, pulmonary function in these mice was not notably different from that of sham-instilled mice. The longitudinal variation in the mean values of the two parameters was found to correlate, suggesting that the time-course of disease progression acted to simultaneously impair both ventilation and gas-exchange function. In addition, the r_a and f_D values were found to correlate significantly on a per mouse basis at week 10, although not prior to week 10, which supports the decision to end the CS and LPS administration at this time-point. Reductions in f_D and increases in the prevalence of ventilation defects have been previously observed using hyperpolarized gas MRI in human COPD patients (34,35), supporting the fact that the CS and LPS model of COPD employed here could successfully induce similar pathological effects to COPD itself. Combining whole-body CS exposure with LPS administration induced significant emphysematous pathology and bronchial wall thickening after 10 weeks of exposure, as illustrated by histology slides (Figures 5 and 6). On the other hand, exposure to only CS has been

Comment [XH16]: R2.2

Comment [XH17]: R1.23&24

reported to typically require ≥ 6 months to establish the characteristic emphysematous pathology in mice (36). While Hansbro et al. succeeded to establish a mouse model of COPD by 8 weeks of CS exposure through the nose only, this procedure required purpose-built equipment that is not readily translatable to our laboratory, and the CS dose was relatively high (2 cigarettes/mouse/day) (37). Thus, our protocol of CS and LPS exposure considerably shortened the time required to produce the two phenotypes of COPD pathology without necessitating specialist equipment. As such, this procedure may be advantageous for future investigations of COPD treatment response.

The present COPD mouse model caused significant decreases of ventilation and gas-exchange parameters: mean r_a of 0.19 ± 0.03 in CS and LPS mice compared with 0.25 ± 0.03 in sham-instilled mice; mean f_D of 4.5 ± 1.0% compared with 6.8 ± 0.6%, respectively, after 10 weeks. The decrease of r_a after 10 weeks of exposure to CS and LPS is indicative of an increase in the bronchial wall thickness, and indeed r_a showed a significant correlation with the histology-derived h value at this time-point (Figure 7). However, the decrease of f_D is indicative of both a reduction in the volume of septal tissue and an increase in the bronchial wall thickness. The decrease in f_D and r_a at the 6 week time-point may be attributable to the increase in bronchial wall thickness, h, (see Supporting Figure S1) since it is unlikely that the volume of septal tissue decreased (as there was no significant change in MLI at the 4 week time-point). This situation may be similar to a previous study in which CS and LPS were administered to rats for 6 weeks (21). According to that report, no histological evidence of COPD (i.e. MLI change) was seen despite overexpression of HMGB1. However, it is worth noting that these observations might not exclude the possibility of early stage emphysema, because mice lack the anatomical characteristics (respiratory bronchioles) for expression of centrilobular emphysema (4). One might also expect that the decrease in

Comment [XH18]: R1.25

Comment [XH19]: R2.2

Comment [XH20]: R1.26

Comment [XH21]: R1.28

f_D was caused in part by a reduction in the volume of the pulmonary capillaries, because the f_D measurement includes a contribution related to blood volume (since ddY-type mice exhibit only a single NMR peak from dissolved-phase ^{129}Xe in lung tissue and blood (31), and furthermore, the XTC technique as employed herein does not enable the distinction of two dissolved-phase ^{129}Xe compartments even if they were present).

In the present study, the efficacy of EP for treatment of the CS and LPS model of COPD was quantified by longitudinal observations of pulmonary function. The reductions in r_a and f_D in the CS and LPS group after 6 weeks recovered to a similar level as the sham-instilled group by 2 and 4 weeks of administration of EP, respectively ($P < 0.01$, see Figures 3 and 4). Because the administration of EP was only started 6 weeks after commencement of CS and LPS exposure (i.e. after some impairment of pulmonary function was observed), EP likely exhibited a combination of both preventative and therapeutic properties in the CS and LPS model of COPD. In other words, EP may have acted to inhibit further emphysema development and to repair the existing bronchial wall damage (Figures 5 and 6). This hypothesis is supported by the lack of significant difference in the r_a and f_D values between 6 and 10 week time-points in the EP-treated group ($P > 0.05$). However, the present study was unable to clarify whether the recovery of HPXe MRI metrics might be indicative of the reparation of tissue loss by early emphysema and/or improved pulmonary hemodynamics. To prove whether EP can indeed act to reverse emphysematous tissue loss, further experiments are needed in which EP administration is started after 10 weeks of CS and LPS exposure.

To the best of our knowledge, this is the first evidence of the therapeutic action of EP in a murine COPD model, as measured by HPXe MRI. Recently, it has been

Comment [XH22]: Reply to editor
R1.3&5
R2.0

Comment [XH23]: R1.29

Comment [XH24]: R2.11

Comment [XH25]: R1.30

reported that intraperitoneal administration of EP can inhibit the expression of HMGB1 (18,19). Additionally, high expression of HMGB1 has been reported to lead to lung functional impairment, and is associated with the development and progression of COPD (20-22). On the other hand, albeit paradoxically, the HMGB1/RAGE pathway is also known to be associated with a series of signalling pathways for tissue repair (23,24). It may be speculated that EP is effective in treating lung diseases caused by chronic inflammation (such as the CS and LPS model of COPD) through the regulation of HMGB1/RAGE, leading to improvement and potentially maintenance of murine pulmonary function. Further studies with corresponding molecular assays are required to substantiate this claim.

CONCLUSION

The feasibility of HPXe MRI for longitudinal assessment of disease progression and pharmacological therapy has been demonstrated in a mouse model of COPD. The model, combining exposure to cigarette smoke and lipopolysaccharide solution, induced COPD characteristics in mice in a relatively short time of 10 weeks and offers potential advantages for pharmacological therapy assessment applications. HPXe MRI-derived metrics of pulmonary function showed considerable impairment in both ventilation and gas-exchange function in CS and LPS mice compared with sham-instilled mice, as verified by histological analysis. Longitudinal HPXe MRI assessment of the action of an anti-inflammatory agent, ethyl pyruvate, for treatment of this COPD model revealed preliminary evidence of its efficacy, and may help to elucidate the exact mechanisms of its therapeutic action in the future.

Comment [XH26]: R1.31

Comment [XH27]: R2.12

Acknowledgements

This work was supported by the Japan Society for the Promotion of Science (JSPS) KAKENHI grant numbers: JP24300163 and JP15H03006. NJS acknowledges funding support from the Medical Research Council (MRC) and the JSPS summer programme (2015).

References

1. Lozano R, Naghavi M, Foreman K, et al. Global and regional mortality from 235 causes of death for 20 age groups in 1990 and 2010: a systematic analysis for the Global Burden of Disease Study 2010. The Lancet 2012;380(9859):2095-2128.
2. Holgate S, Agusti A, Strieter RM, Anderson GP, Fogel R, Bel E, Martin TR, Reiss TF. Drug development for airway diseases: looking forward. Nat Rev Drug Discov 2015;14:367-368.
3. Fricker M, Deane A, Hansbro PM. Animal models of chronic obstructive pulmonary disease. Expert Opin Drug Discov 2014;9(6):629-645.
4. Gardi C, Stringa B, Martorana PA. Animal models for anti-emphysema drug discovery. Expert Opin Drug Discov 2015;10(4):399-410.
5. Mizutani N, Fuchikami J, Takahashi M, Nabe T, Yoshino S, Kohno S. Pulmonary emphysema induced by cigarette smoke solution and lipopolysaccharide in guinea pigs. Biol Pharm Bull 2009;32:1559-1564.
6. Li JJ, Wang W, Baines KJ, Bowden NA, Hansbro PM, Gibson PG, Kumar RK, Foster PS, Yang M. IL-27/IFN-γ induce MyD88-dependent steroid-resistant airway hyperresponsiveness by inhibiting glucocorticoid signaling in macrophages. J Immunol 2010;185(7):4401-4409.
7. Fain SB, Korosec FR, Holmes JH, O'Halloran R, Sorkness RL, Grist TM. Functional lung imaging using hyperpolarized gas MRI. J Magn Reson Imag 2007;25(5):910-923.
8. Mugler JP, III, Altes TA. Hyperpolarized ^{129}Xe MRI of the human lung. J Magn Reson Imag 2013;37(2):313-331.
9. van Beek EJR, Wild JM, Kauczor H-U, Schreiber W, Mugler JP, de Lange EE. Functional MRI of the lung using hyperpolarized 3-helium gas. J Magn Reson Imag

2004;20(4):540-554.

10. Kirby M, Pike D, Coxson HO, McCormack DG, Parraga G. Hyperpolarized ^{3}He ventilation defects used to predict pulmonary exacerbations in mild to moderate chronic obstructive pulmonary disease. Radiology 2014;273(3):887-896.
11. Qing K, Mugler JP 3rd, Altes TA, Jiang Y, Mata JF, Miller GW, Ruset IC, Hersman FW, Ruppert K. Assessment of lung function in asthma and COPD using hyperpolarized ^{129}Xe chemical shift saturation recovery spectroscopy and dissolved-phase MRI. NMR Biomed 2014;27(12):1490-1501.
12. Imai H, Kimura A, Fujiwara H. Small animal imaging with hyperpolarized ^{129}Xe magnetic resonance. Anal Sci 2014;30(1):157-166.
13. Tetsumoto S, Takeda Y, Imai H, et al. Validation of noninvasive morphological and diffusion imaging in mouse emphysema by micro-computed tomography and hyperpolarized ^{129}Xe magnetic resonance imaging. Am J Respir Cell Mol Biol 2013;49(4):592-600.
14. Kung CW, Lee YM, Cheng PY, Peng YJ, Yen MH. Ethyl pyruvate reduces acute lung injury via regulation of iNOS and HO-1 expression in endotoxemic rats. J Surg Res 2011;167(2):e323-e331.
15. Liu C, Fang C, Cao G, Liu K, Wang B, Wan Z, Li S, Wu S. Ethyl pyruvate ameliorates monocrotaline-induced pulmonary arterial hypertension in rats. J Cardiovasc Pharmacol 2014;64(1):7-15.
16. Shang GH, Lin DJ, Xiao W, Jia CQ, Li Y, Wang AH, Dong L. Ethyl pyruvate reduces mortality in an endotoxin-induced severe acute lung injury mouse model. Respir Res 2009;10:91.
17. Pulathan Z, Altun G, Hemşinli D, Menteşe A, Yuluğ E, Civelek A. Role of ethyl pyruvate in systemic inflammatory response and lung injury in an experimental

model of ruptured abdominal aortic aneurysm. Biomed Res Int 2014;2014:857109.

18. Cheng P, Dai W, Wang F, Lu J, Shen M, Chen K, Li J, Zhang Y, Wang C, Yang J, Zhu R, Zhang H, Zheng Y, Guo C-Y, Xu L. Ethyl pyruvate inhibits proliferation and induces apoptosis of hepatocellular carcinoma via regulation of the HMGB1–RAGE and AKT pathways. Biochem Biophys Res Commun 2014;443(4):1162-1168.
19. Lee YM, Kim J, Jo K, Shin SD, Kim C-S, Sohn EJ, Kim SG, Kim JS. Ethyl Pyruvate Inhibits Retinal Pathogenic Neovascularization by Downregulating HMGB1 Expression. J Diabetes Res 2013;2013:8.
20. Ko H-K, Hsu W-H, Hsieh C-C, Lien T-C, Lee T-S, Kou YR. High expression of high-mobility group box 1 in the blood and lungs is associated with the development of chronic obstructive pulmonary disease in smokers. Respirology 2014;19(2):253-261.
21. Wang CM, Jiang M, Wang HJ. Effect of NF-κB inhibitor on high-mobility group protein B1 expression in a COPD rat model. Mol Med Rep 2013;7(2):499-502.
22. Zhang Y, Li S, Wang G, Han D, Xie X, Wu Y, Xu J, Lu J, Li F, Li M. Changes of HMGB1 and sRAGE during the recovery of COPD exacerbation. J Thorac Dis 2014;6(6):734-741.
23. Lee DE, Trowbridge RM, Ayoub NT, Agrawal DK. High-mobility Group Box Protein-1, Matrix Metalloproteinases, and Vitamin D in Keloids and Hypertrophic Scars. Plast Reconstr Surg Glob Open 2015;3(6):e425.
24. Pandolfi F, Altamura S, Frosali S, Conti P. Key Role of DAMP in Inflammation, Cancer, and Tissue Repair. Clin Ther 2016;38(5):1017-1028.
25. Walker TG, Happer W. Spin-exchange optical pumping of noble-gas nuclei. Reviews of Modern Physics 1997;69(2):629-642.
26. Imai H, Fukutomi J, Kimura A, Fujiwara H. Effect of reduced pressure on the

polarization of ^{129}Xe in the production of hyperpolarized ^{129}Xe gas: Development of a simple continuous flow mode hyperpolarizing system working at pressures as low as 0.15 atm. Concepts in Magnetic Resonance Part B: Magnetic Resonance Engineering 2008;33B(3):192-200.

27. Imai H, Kimura A, Hori Y, Iguchi S, Kitao T, Okubo E, Ito T, Matsuzaki T, Fujiwara H. Hyperpolarized ^{129}Xe lung MRI in spontaneously breathing mice with respiratory gated fast imaging and its application to pulmonary functional imaging. NMR Biomed 2011;24:1343-1352.
28. Imai H, Matsumoto H, Miyakoshi E, Okumura S, Fujiwara H, Kimura A. Regional fractional ventilation mapping in spontaneously breathing mice using hyperpolarized ^{129}Xe MRI. NMR Biomed 2015;28:24-29.
29. Hamedani H, Clapp JT, Kadlecek SJ, Emami K, Ishii M, Gefter WB, Xin Y, Cereda M, Shaghaghi H, Siddiqui S, Rossman MD, Rizi RR. Regional Fractional Ventilation by Using Multibreath Wash-in ^{3}He MR Imaging. Radiology 2016;279(3):917-924.
30. Ruppert K, Brookeman JR, Hagspiel KD, Mugler JP, III. Probing lung physiology with xenon polarization transfer contrast (XTC). Magn Reson Med 2000;44(3):349-357.
31. Imai H, Kimura A, Iguchi S, Hori Y, Masuda S, Fujiwara H. Non-invasive Detection of Pulmonary Tissue Destruction in a Mouse Model of Emphysema Using Hyperpolarized ^{129}Xe MRS under Spontaneous Respiration. Magn Reson Med 2010;64(4):929-938.
32. Hardaker EL, Freeman MS, Dale N, Bahra P, Raza F, Banner KH, Poll C. Exposing rodents to a combination of tobacco smoke and lipopolysaccharide results in an exaggerated inflammatory response in the lung. Br J Pharmacol

2010;160(8):1985-1996.

33. Song HH, Shin IS, Woo SY, Lee SU, Sung MH, Ryu HW, Kim DY, Ahn KS, Lee HK, Lee D, Oh SR. Piscroside C, a novel iridoid glycoside isolated from Pseudolysimachion rotundum var. subinegrum suppresses airway inflammation induced by cigarette smoke. J Ethnopharmacol 2015;170:20-27.
34. Dregely I, Mugler JP, III, Ruset IC, Altes TA, Mata JF, Miller GW, Ketel J, Ketel S, Distelbrink J, Hersman FW, Ruppert K. Hyperpolarized Xenon-129 gas-exchange imaging of lung microstructure: first case studies in subjects with obstructive lung disease. J Masgn Reson Imag 2011;33(5):1052-1062.
35. Kirby M, Svenningsen S, Owrangi A, Wheatley A, Farag A, Ouriadov A, Santyr GE, Etemad-Rezai R, Coxson HO, McCormack DG, Parraga G. Hyperpolarized ^{3}He and ^{129}Xe MR Imaging in Healthy Volunteers and Patients with Chronic Obstructive Pulmonary Disease. Radiology 2012;265(2):600-610.
36. Churg A, Cosio M, Wright JL. Mechanisms of cigarette smoke-induced COPD: insights from animal models. Am J Physiol Lung Cell Mol Physiol 2008;294(4):L612-631.
37. Beckett EL, Stevens RL, Jarnicki AG, et al. A new short-term mouse model of chronic obstructive pulmonary disease identifies a role for mast cell tryptase in pathogenesis. J Allergy Clin Immunol 2013;131(3):752-762.

Figure legends:

Figure 1. Example parametric maps of r_a derived from longitudinal studies of mice in each of the three groups, from top to bottom: sham-instilled; CS and LPS model of COPD; EP-treated. In all cases, the time course is shown horizontally.

Figure 2. Example parametric maps of f_D derived from longitudinal studies of mice in each of the three groups, from top to bottom: sham-instilled; CS and LPS model of COPD; EP-treated. In all cases, the time course is shown horizontally.

Figure 3. Box plots of the temporal change of mean r_a values for all mice, separated by group. Significant differences between groups are indicated by solid lines, along with the corresponding p values of significance (*$P < 0.05$; ** $P < 0.01$).

Figure 4. Box plots of the temporal change of mean f_D values for all mice, separated by group. Significant differences between groups are indicated by solid lines, along with the corresponding p values of significance (*$P < 0.05$; ** $P < 0.01$).

Figure 5. a) Box plots showing the mean MLI values obtained from mice in each of the four groups, from left to right: sham-instilled; histological analysis (CS&LPS 4w), CS and LPS model of COPD (CS&LPS10w); EP-treated. b) Representative examples of

H&E stained histology slides obtained from 5 lung regions of one mouse chosen from each of the four groups. RU, right upper lobe; RM, right middle lobe; RL, right lower lobe; LU, upper region of the left lobe; LL, lower region of the left lobe. Note: mean values in a) represent the mean of the whole group; mean values in b) represent the mean for the selected mouse from each group.

Figure 6. a) Box plots showing the mean bronchial wall thickness (h) values obtained from mice in each of the four groups, from left to right: sham-instilled; histological analysis (CS&LPS 4w), CS and LPS model of COPD (CS&LPS10w); EP-treated after the 10 week experimental protocol. b) Representative examples of H&E stained histology slides obtained from the four groups.

Figure 7. Relationships between HPXe MRI-derived parameters of pulmonary function (r_a and f_D), and histology-derived parameters of lung structure (MLI and h) obtained from the sham-instilled (□), EP-treated (○), and CS and LPS (▲) mice after the 10 week experimental protocol. The Pearson's r value and P value of statistical significance are noted in each plot.

Supporting Figure S1. a) Box plots showing the mean bronchial wall thickness (*h*) values obtained from mice in each of the five groups, from left to right: sham-instilled; histological analysis (CS&LPS 4w and CS&LPS 6w), CS and LPS model of COPD (CS&LPS10w); EP-treated after the 10 week experimental protocol. b) Representative examples of H&E stained histology slides obtained from the five groups.

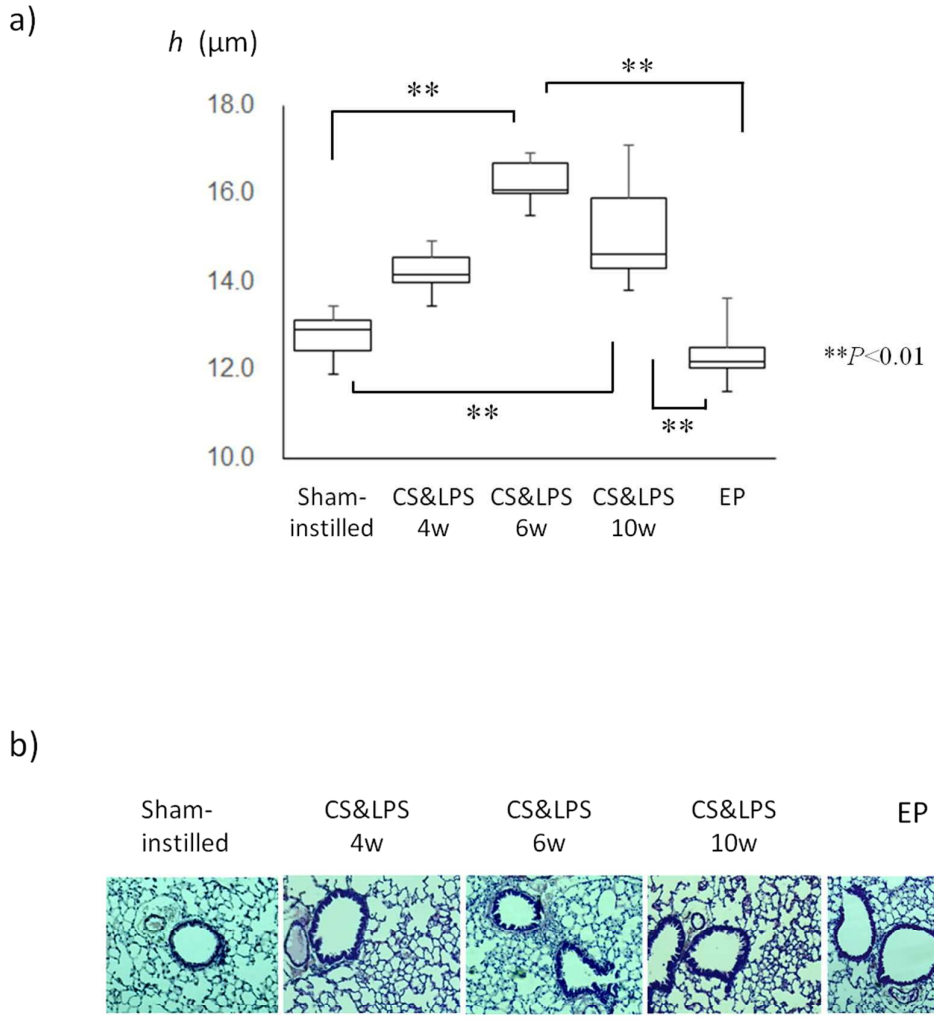

Supporting Figure S1. a) Box plots showing the mean bronchial wall thickness (*h*) values obtained from mice in each of the five groups, from left to right: sham-instilled; histological analysis (CS&LPS 4w and CS&LPS 6w), CS and LPS model of COPD (CS&LPS10w); EP-treated after the 10 week experimental protocol. b) Representative examples of H&E stained histology slides obtained from the five groups.

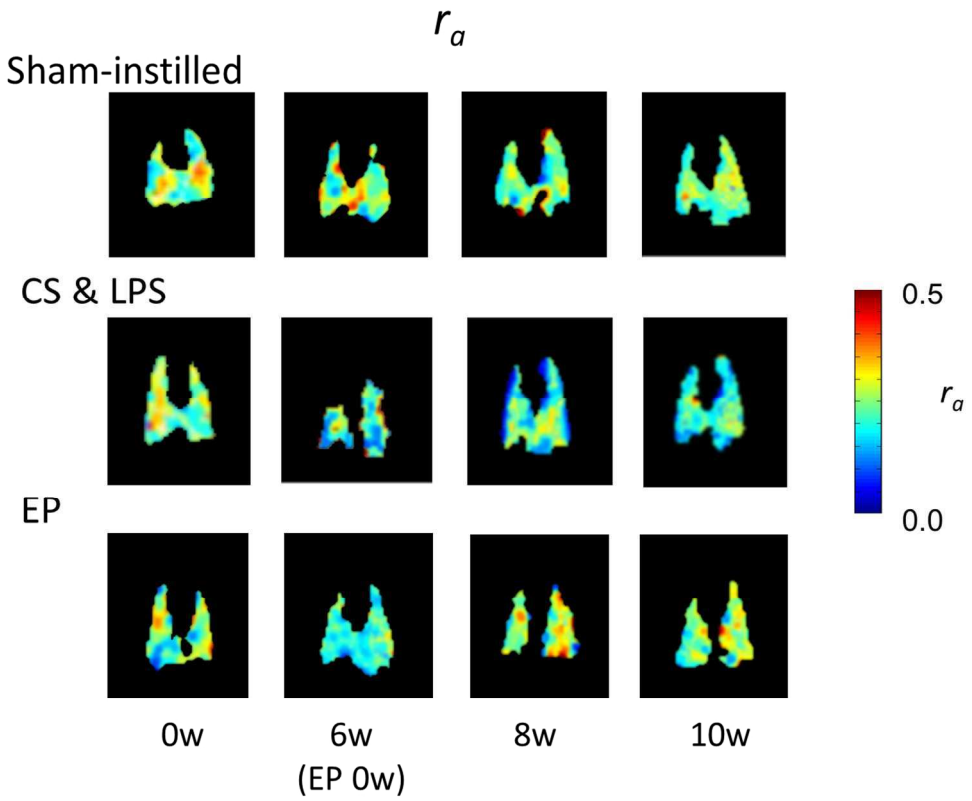

Figure 1. Example parametric maps of ra derived from longitudinal studies of mice in each of the three groups, from top to bottom: sham-instilled; CS and LPS model of COPD; EP-treated. In all cases, the time course is shown horizontally.

118x118mm (300 x 300 DPI)

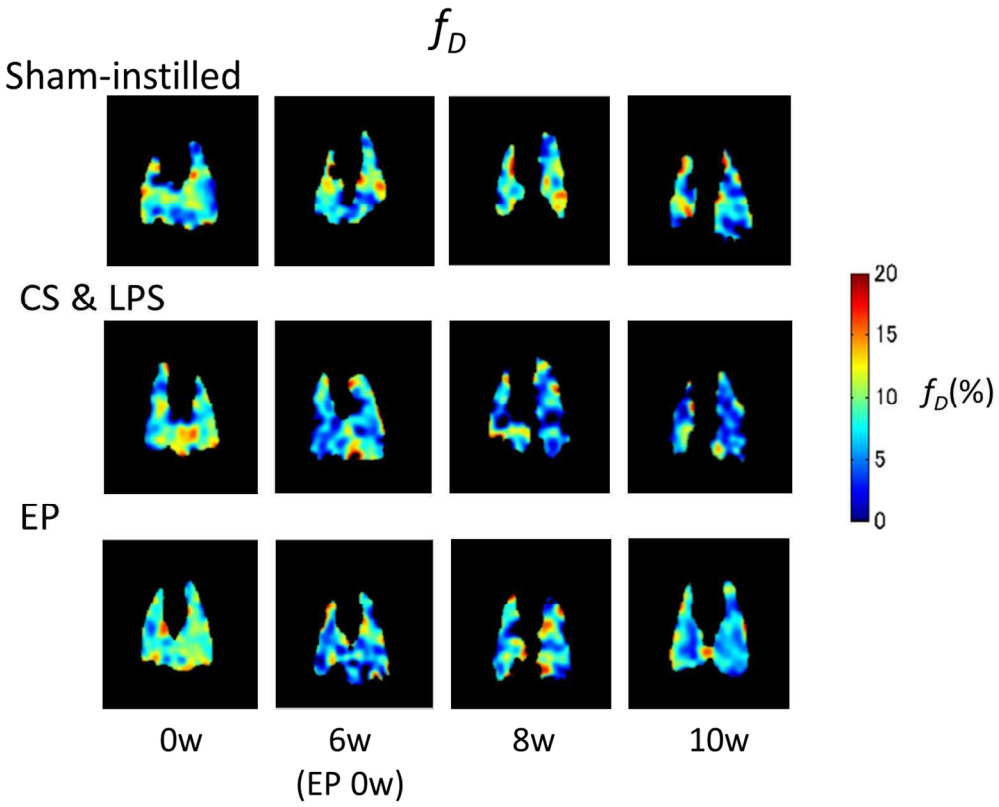

Figure 2. Example parametric maps of fD derived from longitudinal studies of mice in each of the three groups, from top to bottom: sham-instilled; CS and LPS model of COPD; EP-treated. In all cases, the time course is shown horizontally.

118x118mm (300 x 300 DPI)

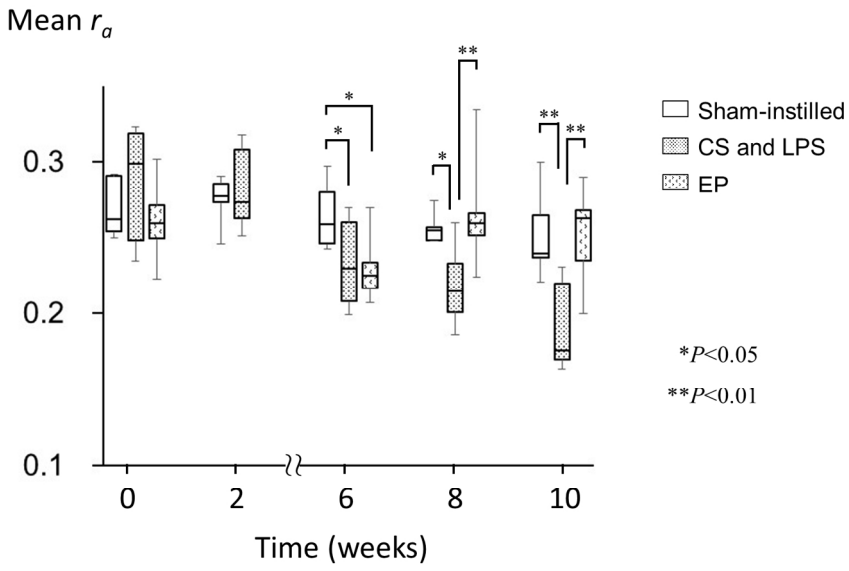

Figure 3. Box plots of the temporal change of mean ra values for all mice, separated by group. Significant differences between groups are indicated by solid lines, along with the corresponding p values of significance (*P < 0.05; ** P < 0.01).

152x152mm (300 x 300 DPI)

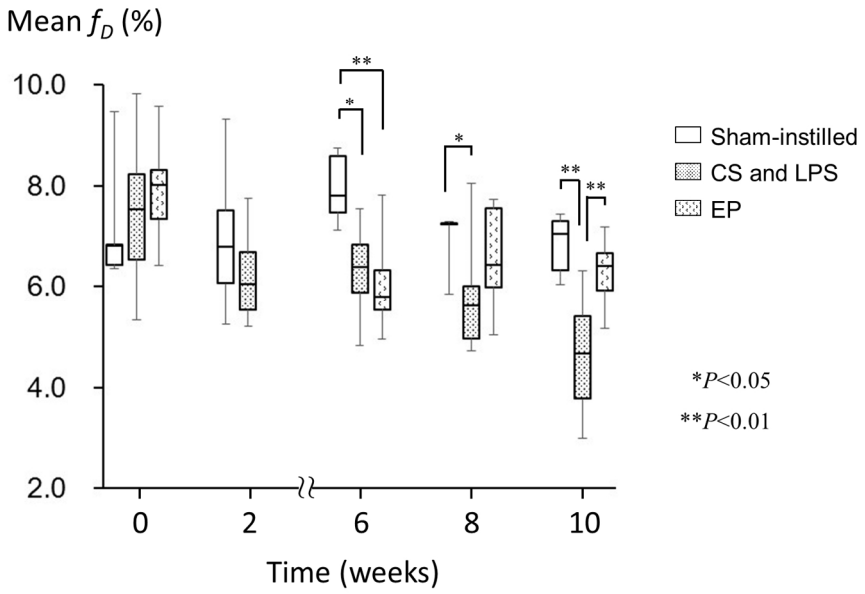

Figure 4. Box plots of the temporal change of mean fD values for all mice, separated by group. Significant differences between groups are indicated by solid lines, along with the corresponding p values of significance (*P < 0.05; ** P < 0.01).

152x152mm (300 x 300 DPI)

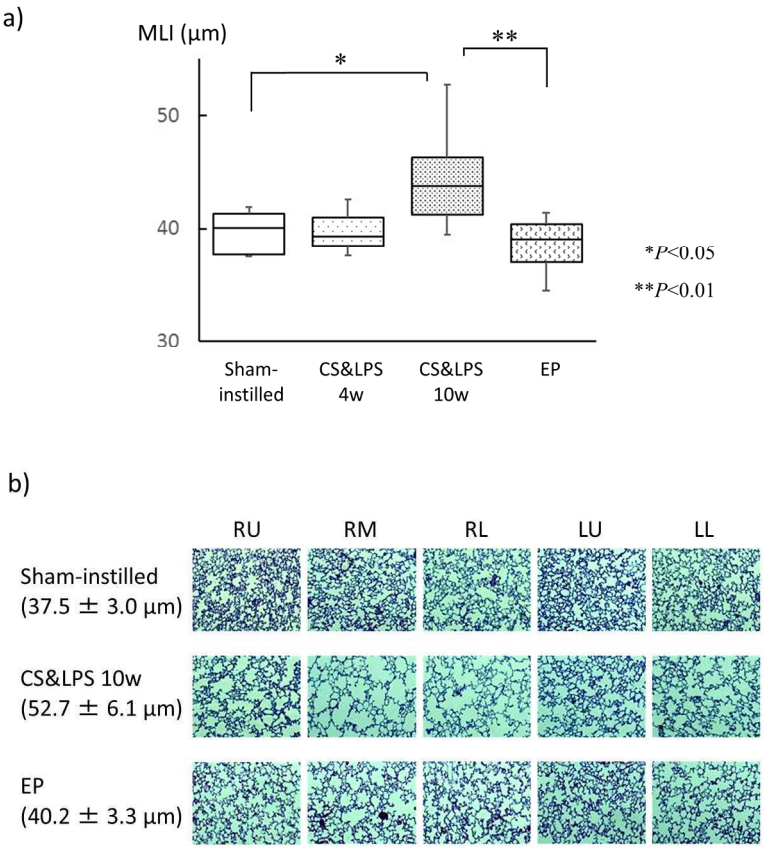

Figure 5. a) Box plots showing the mean MLI values obtained from mice in each of the four groups, from left to right: sham-instilled; histological analysis (CS&LPS 4w), CS and LPS model of COPD (CS&LPS10w); EP-treated. b) Representative examples of H&E stained histology slides obtained from 5 lung regions of one mouse chosen from each of the four groups. RU, right upper lobe; RM, right middle lobe; RL, right lower lobe; LU, upper region of the left lobe; LL, lower region of the left lobe. Note: mean values in a) represent the mean of the whole group; mean values in b) represent the mean for the selected mouse from each group.

203x203mm (300 x 300 DPI)

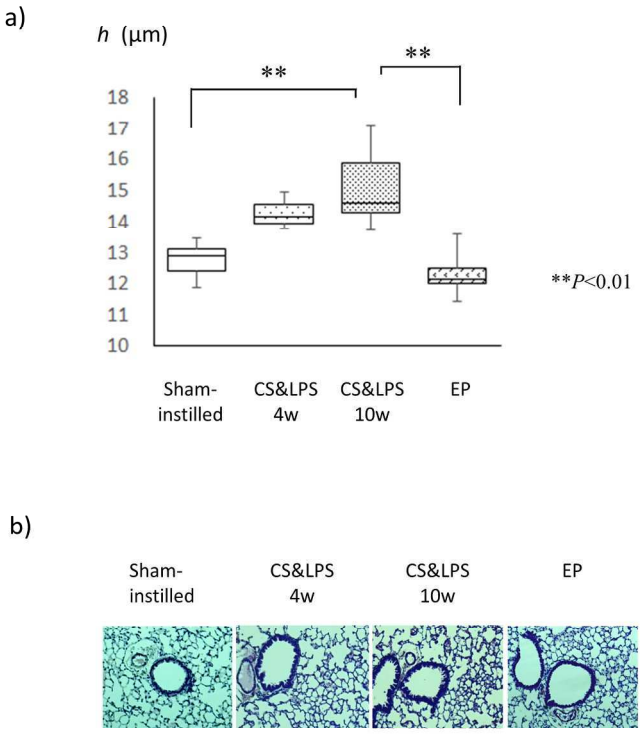

Figure 6. a) Box plots showing the mean bronchial wall thickness (h) values obtained from mice in each of the four groups, from left to right: sham-instilled; histological analysis (CS&LPS 4w), CS and LPS model of COPD (CS&LPS10w); EP-treated after the 10 week experimental protocol. b) Representative examples of H&E stained histology slides obtained from the four groups.

203x203mm (300 x 300 DPI)

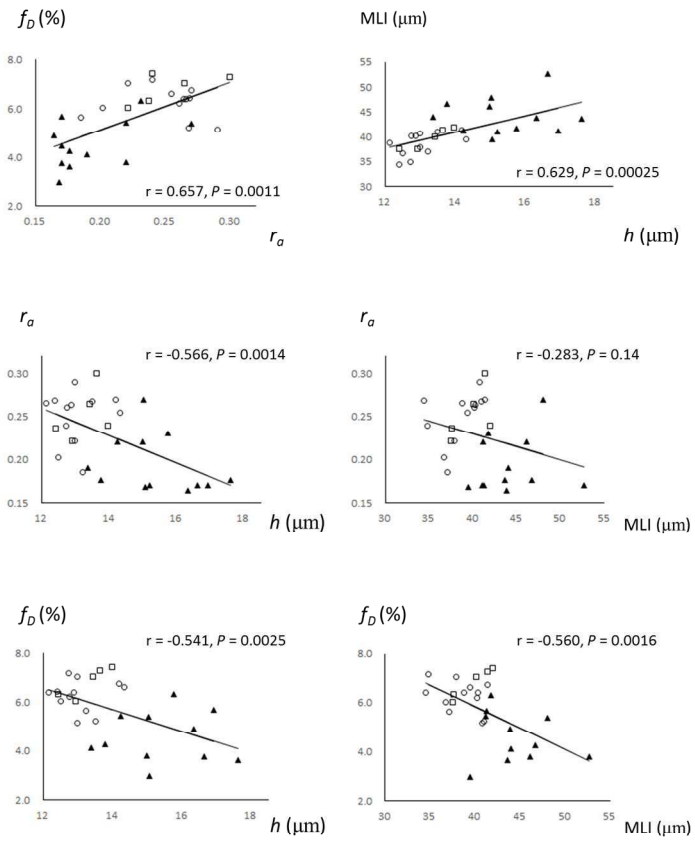

Figure 7. Relationships between HPXe MRI-derived parameters of pulmonary function (ra and fD), and histology-derived parameters of lung structure (MLI and h) obtained from the sham-instilled (□), EP-treated (○), and CS and LPS (▲) mice after the 10 week experimental protocol. The Pearson's r value and P value of statistical significance are noted in each plot.

152x152mm (300 x 300 DPI)